

Atomic-scale structural and electronic properties of SrTiO₃/GaAs interfaces: A combined STEM-EELS and first-principles study

Liang Hong,¹ Kunal Bhatnagar,² Ravi Droopad,² Robert F. Klie,¹ and Serdar Ögüt¹

¹*Department of Physics, University of Illinois at Chicago, Chicago, Illinois 60607, USA*

²*Ingram School of Engineering, Texas State University, San Marcos, Texas 78666, USA*

(Received 1 May 2017; published 26 July 2017)

The electronic properties of epitaxial oxide thin films grown on compound semiconductors are largely determined by the interfacial atomic structure, as well as the thermodynamic conditions during synthesis. Ferroelectric polarization and Fermi-level pinning in SrTiO₃ films have been attributed to the presence of oxygen vacancies at the oxide/semiconductor interface. Here, we present scanning transmission electron microscopy (STEM) and electron energy-loss spectroscopy analyses of GaAs films grown on SrTiO₃ combined with first-principles calculations to determine the atomic and electronic structures of the SrTiO₃/GaAs interfaces. An atomically abrupt SrO/As interface is observed and the interfacial SrO layer is found to be O-deficient. First-principles density functional theory (DFT) calculations show SrO/Ga and Sr/As interfaces are favorable under O-rich and O-poor conditions, respectively. The SrO/Ga interface is reconstructed via the formation of Ga-Ga dimers while the Sr/As interface is abrupt and consistent with the experiment. DFT calculations further reveal that intrinsic two-dimensional electron gas (2DEG) forms in both SrO/Ga and Sr/As interfaces, and the Fermi level is pinned to the localized 2DEG states. Interfacial O vacancies can enhance the 2DEG density while it is possible for Ga/As vacancies to unpin the Fermi level from the 2DEG states.

DOI: [10.1103/PhysRevB.96.035311](https://doi.org/10.1103/PhysRevB.96.035311)

I. INTRODUCTION

The properties of a hybrid thin film heterostructure are often dominated by the interface between the materials that comprise the structure. Extensive research has revealed key mechanisms and material properties that control an interface between chemically similar, isostructural materials. Integrating thin films with dramatically dissimilar chemical bonding, crystal symmetries, and electronic structures represents a promising new approach to engineering novel functional materials. For example, ultrathin SrTiO₃ (STO) films grown on Si or GaAs that exhibit ferroelectric properties can facilitate the implementation of optical nonlinearities and carrier modulation at extremely high carrier densities. Successful integration of a STO thin film on a Si substrate was first demonstrated by McKee *et al.* [1]. Compared to Si, compound semiconductors, such as GaAs, have much higher electron mobility and a wider and direct band gap, making them promising for applications in electronics and photonics by directly coupling the polarization of a ferroelectric to the properties of a semiconductor. Perovskite oxide thin films, exhibiting enormous optical nonlinearities, can, therefore, serve as a key component for hybrid semiconductor-photonics systems. However, deposition of perovskite oxides directly with semiconductors is challenging due to the structural difference and the potential oxidation of the semiconductor surface [2]. Since the stability and performance of these heterojunctions are often governed by atomic-scale defects and interfaces between the two dissimilar materials, an understanding of the interfacial structural and electronic properties is critical.

The STO/GaAs heterointerfaces have been studied both theoretically and experimentally during the last decade [3–15]. The STO thin film was epitaxially deposited on GaAs (001) without any amorphous interfacial layer using the molecular beam epitaxy (MBE) method by Liang *et al.* [3,4]. A Ti prelayer was used to facilitate the growth of STO on a GaAs

substrate. The epitaxial STO thin film was found to be rotated by 45° with respect to GaAs so that the lattice mismatch between STO ($a_{\text{STO}} = 3.905 \text{ \AA}$) and GaAs ($a_{\text{GaAs}}/\sqrt{2} = 3.997 \text{ \AA}$) can be minimized to 2.3%. The STO/GaAs interfaces were then characterized using scanning transmission electron microscopy (STEM) imaging at atomic resolution by Klie *et al.* [5]. It was reported that SrO-terminated STO film is epitaxially grown on As-terminated GaAs with atomically sharp interfaces. In addition, STO thin films deposited with and without Ti prelayer on GaAs have structurally identical interfaces. A more detailed characterization of the atomic and electronic structures of the STO/GaAs interfaces was carried out by Qiao *et al.* [6] using low-energy electron energy-loss spectroscopy (EELS) along with first-principles calculations. By analyzing the O vacancies and Ti concentrations in the STO film and across the interface, it was suggested that without the presence of a Ti prelayer, the interfacial As gets oxidized, which results in Fermi-level pinning, while in the presence of the Ti prelayer, Ti diffuses into GaAs and alleviates the oxidation which unpins the Fermi level. From a computational perspective, there have been few first-principles total energy calculations performed using density functional theory (DFT) to determine the stable structures of the STO/GaAs interfaces. By comparing the formation energies of various interface configurations, the SrO/Ga heterostructure with Ga-O bonds was found to be the most favorable [12–15], which is consistent with the recent x-ray photoemission spectroscopy characterization of the STO/GaAs interface [9] but inconsistent with previous STEM works [5,6]. However, a more systematic and detailed study with a combination of experimental and theoretical investigations is needed to determine the structure of the STO/GaAs interface. Since GaAs (001) was used experimentally as a substrate with fixed As termination in the previous STEM-EELS studies, it was not possible to determine the energetic preference of Ga or

As termination at the interface. This can be potentially solved by depositing GaAs films on STO, which was achieved more than a decade ago by Droopad *et al.* [16,17], but the atomic structure of this heterointerface has not yet been characterized. In addition, the effects of atomic-scale interfacial defects on the electronic properties of the heterostructure, including Fermi-level pinning and band alignment, need to be studied to establish a better understanding of the structure-property relationship of the STO/GaAs interface.

In this work, we present results and analyses of a combined experimental and theoretical study of the STO/GaAs heterointerfaces at the atomic scale. Epitaxial GaAs is grown on a Si substrate with a STO buffer layer using the MBE method. The STO/GaAs interface in our sample is characterized using atomic-resolution STEM imaging and EELS. (2×2) structural models with various interface compositions are constructed and optimized using first-principles DFT calculations. Our results show that an O-deficient SrO layer in contact with an As layer is the most favorable interface structure, and the experimentally observed interface structure is reproduced in the DFT simulation. Ga termination is favored over As termination at the interface under O-rich conditions, but the GaAs surface is easily oxidized by forming a Ga_2O_3 interlayer. The interface structure is determined by the accommodation of polar discontinuity, which is related to the interface composition. Interfacial vacancies are found to play an important role in determining the electronic properties of the heterointerfaces. The rest of the paper is organized as follows. In Sec. II, we discuss the technical details of the experimental and theoretical methods used in this work. In Sec. III, we present both experimental and theoretical results and analyses of the STO/GaAs interfaces, including their energetics, atomic and electronic structures, and the effect of interfacial vacancies. Finally, our results are summarized in Sec. IV.

II. METHODS

A. Experimental methods

The sample used in this work is grown using the MBE method. A 10-nm-thick SrO-terminated STO thin film is grown on a Si (001) wafer with a 4° miscut in the [110] direction. During the growth, oxygen diffuses through the perovskite STO layer and reacts with the interfacial Si atoms forming a SiO_2 interlayer. The SrO termination of the STO film is achieved by closing the shutter of the Ti effusion cell while keeping that of the Sr effusion cell open in the oxide MBE chamber. The wafer is then transferred into a second MBE chamber for the growth of a III-V semiconductor layer. Simultaneous Ga and As_2 are exposed to the STO surface to form a 1- μm -thick epitaxial GaAs layer. More details about the MBE growth are presented in the Supplemental Material [18].

Two cross-section samples are polished in two directions that are 90° rotated with respect to each other using standard wedge polishing methods and then thinned down to electron transparency (<50 nm) using low-energy (0.5–3 kV) and low-angle (6° – 10°) argon ion milling on a liquid-nitrogen-cooled stage to minimize the ion beam damage.

The experimental characterization data are obtained using the aberration-corrected JEOL JEM-ARM200CF scanning transmission electron microscopy (STEM) equipped with a

cold field-emission source, which yields an energy resolution of 0.35 eV, and a probe spherical-aberration corrector which allows for 78-pm spatial resolution using an acceleration voltage of 200 kV [24]. The high-angle annular dark-field (HAADF) images are acquired at 200 kV with a convergence semiangle of 29 mrad and a collection angle from 90 to 170 mrad. The atomic-resolution HAADF images are recorded at a magnification of 2×10^7 (pixel size of 0.02 nm) and pixel dwell time of 31 μs . For EELS at 200 kV, a convergence angle of 30 mrad and a collection angle with 35 mrad are used. Energy dispersions of 0.1 eV/channel and 0.3 eV/channel are used for the measurement of the Ti $L_{3,2}$ -edge and the O K -edge, respectively. The atomic-resolution EELS line scan is recorded using pixel size of 0.06 nm and pixel dwell time of 0.5–0.7 s. The exponential EEL spectrum background is subtracted from each spectrum and the resulting data are normalized with respect to the post edge intensity. No obvious beam damage to the sample is observed during both imaging and EELS collection at 200 kV.

B. Theoretical methods

First-principles calculations are carried out within the framework of DFT using the projector-augmented wave method [25], as implemented in Vienna *Ab Initio* Simulation Package (VASP) [26], and the exchange-correlation

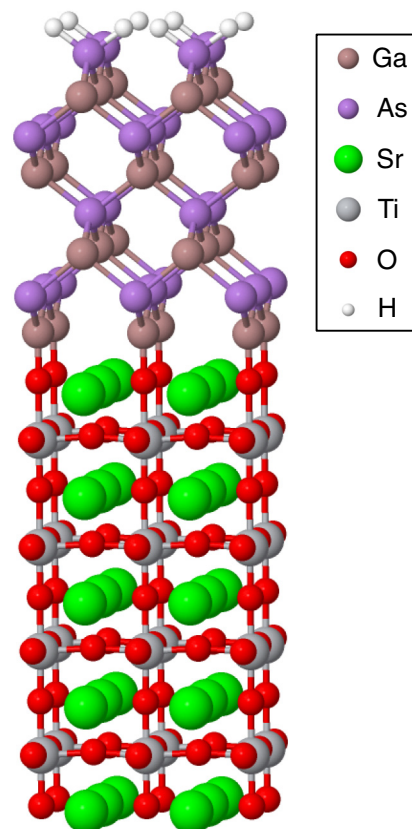


FIG. 1. Ball-and-stick model of the (2×2) STO/GaAs interfaces in three-dimensional view. The top surface of GaAs is passivated by pseudohydrogen atoms and the bottom surface of STO is in contact with vacuum.

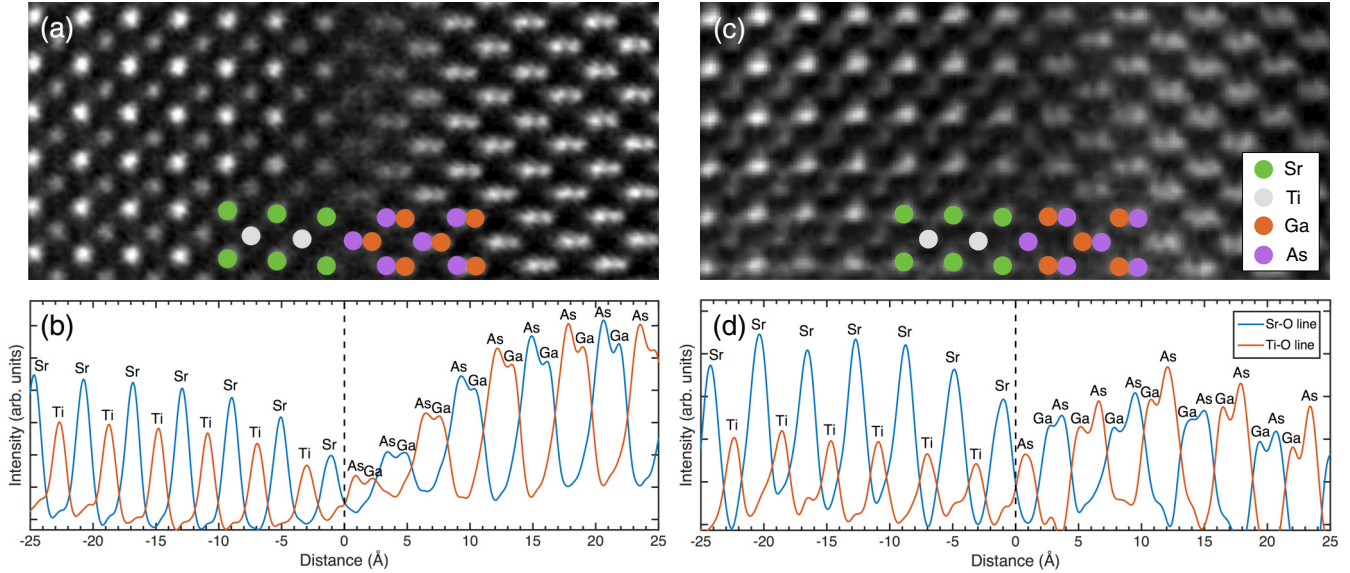


FIG. 2. Atomic-resolution HAADF images of the STO/GaAs interface from two different views which are 90° rotated: (a) the STO [010]||GaAs [110] epitaxy with full GaAs dumbbell structure at the interface and (c) the STO [100]||GaAs [1 $\bar{1}$ 0] epitaxy with half GaAs dumbbell structure at the interface. The images are taken from dislocation-free areas and filtered using average background subtraction filter within a Gatan Digital Micrograph. Panels (b) and (d) show the intensity profiles of atomic lines centered on the Sr and Ti in STO averaged from (a) and (c), respectively.

functional of Perdew-Burke-Ernzerhof (PBE) [27]. The plane-wave energy cutoff is set as 400 eV. Periodic slabs with (2×2) surface cell, as shown in Fig. 1, are constructed to simulate the STO/GaAs interfaces. The slabs are fully optimized with a maximum force criterion of 10^{-2} eV/Å. $4 \times 4 \times 1$ and $12 \times 12 \times 1$ Monkhorst-Pack k -point grids are used during structural optimization and density of states (DOS) calculations, respectively.

The computed lattice parameters of bulk STO and GaAs are found to be 3.94 and 5.76 Å, respectively. To mimic GaAs growth on STO substrate, we use an in-plane lattice parameter of $a_{\text{GaAs}} = 5.57$ Å ($=\sqrt{2}a_{\text{STO}}$) for GaAs, with a 45° in-plane rotation, to match the lattice parameter of STO. The top surface of GaAs is the As layer and is passivated with pseudohydrogens to saturate the As dangling bonds [28]. The bottom surface of STO is SrO layer in contact with an out-of-plane vacuum of 8 Å to separate the slabs. The electronic and structural properties of the slabs are well converged with respect to both the k -point sampling and the length of vacuum. Various interface structures, including SrO- or TiO_2 -terminated STO and bare Sr- or Ti-terminated STO in contact with Ga- or As-terminated GaAs, are constructed to investigate the STO/GaAs interfacial registry. We use the notation SrO/Ga (Sr/Ga) to denote the interface of fully oxygenated (O-deficient) SrO-terminated STO in contact with Ga-terminated GaAs. Considering all the terminations, we have eight different interfacial configurations, which are SrO/Ga, TiO_2 /Ga, SrO/As, TiO_2 /As, Sr/Ga, Ti/Ga, Sr/As, and Ti/As.

The formation energy for a given interfacial configuration is defined as [29]

$$E_{\text{interface}} = E_{\text{slab}} - n_{\text{Sr}}\mu_{\text{Sr}} - n_{\text{Ti}}\mu_{\text{Ti}} - n_{\text{O}}\mu_{\text{O}} - n_{\text{Ga}}\mu_{\text{Ga}} - n_{\text{As}}\mu_{\text{As}}, \quad (1)$$

where E_{slab} is the total energy of the corresponding slab, n_i ($i = \text{Sr}, \text{Ti}, \text{O}, \text{Ga}, \text{and As}$) is the number of atoms or units of type i in the slab, and μ_i is the corresponding chemical potential. The chemical potentials in Eq. (1) are subject to the constraints of equilibrium with bulk STO and GaAs. Additional constraints are used to prevent formation of secondary phases including TiO_2 , Ti_2O_3 , $\text{Sr}_6\text{Ti}_5\text{O}_{16}$, and Ga_2O_3 [12,30,31]. More details about the proposed interface structures, constraints of chemical potentials, and band alignment are presented in the Supplemental Material [18].

III. RESULTS AND DISCUSSION

A. Experimental characterization of the interface

The atomic-resolution HAADF images of our sample taken from cross sections in two directions that are rotated 90° with respect to each other are displayed in Fig. 2. Figure 2(a), with STO [010]||GaAs [110] epitaxy, shows full GaAs dumbbell structure at the interface, while Fig. 2(c), with STO [100]||GaAs [1 $\bar{1}$ 0] epitaxy, shows half GaAs dumbbell structure at the interface. Both images exhibit a sharp interface between STO and GaAs in $1 \times$ periodicity without any surface reconstruction or amorphous interlayer. The elements can be characterized by the intensity contrast of each atomic column in the HAADF images since the HAADF intensity is directly correlated to the atomic number. From the intensity line profiles shown in Figs. 2(b) and 2(d), we can clearly see that STO films are terminated by the SrO layer while GaAs is terminated by As. The interfacial As atoms are located above the oxygen sites in the SrO, and the GaAs dumbbells are in excellent epitaxy with respect to SrO or TiO_2 columns in the out-of-plane direction.

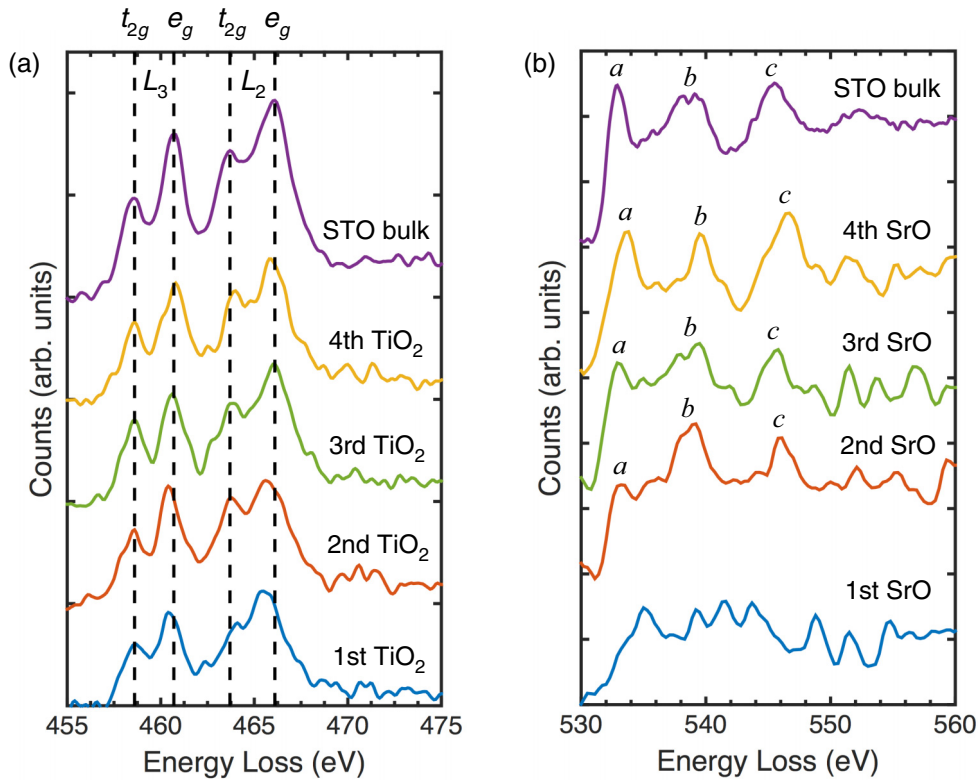


FIG. 3. (a) EEL spectra of a Ti $L_{3,2}$ -edge taken from the STO bulk and the first to fourth TiO_2 layers near the STO/GaAs interface. The dashed lines denote the positions of the four peaks in the bulk spectrum. (b) The O K -edge taken from the STO bulk and the first to fourth SrO layers near the STO/GaAs interface. The spectrum data are smoothed using a Gaussian function.

For Ti oxides, it is known that the energy-loss near-edge fine structures in the Ti $L_{3,2}$ -edge can reflect the valence state, coordination, and site geometry of Ti [32], providing fundamental information on cation ordering and defect clustering such as O vacancies [33]. Therefore, atomic-resolution EEL spectra of Ti $L_{3,2}$ -edge are taken from the first four TiO_2 layers at the STO/GaAs interface and compared with that in bulk STO to examine the near-interface Ti valence and O concentration. As shown in Fig. 3(a), the Ti $L_{3,2}$ -edge of the second to fourth TiO_2 layers exhibit four prominent peaks originating from the splitting of $3d^0$ states into t_{2g} and e_g components, which corresponds to a Ti^{4+} valence. In the first TiO_2 layer, the intensity of the t_{2g} peaks significantly decreases and the positions of e_g peaks shift to lower energies, which indicates a decrease of Ti valence from $4+$ to a mixture of $3+$ and $4+$ [33,34]. The decrease of Ti valence near the interface can be attributed to the interfacial O vacancies. Moreover, the t_{2g} - e_g splitting in both the L_3 and the L_2 edges reduces near the interface compared to the bulk spectrum, as a result of the increased TiO_6 octahedral distortion due to O vacancies and the ferroelectric polarization induced by the polar GaAs (001) surface.

To further confirm the interfacial O vacancies, atomic-resolution EEL spectra of the O K -edge are taken from the first four SrO layers at the STO/GaAs interface. In Fig. 3(b), it is clearly noticeable that the near-edge fine structure of the O K -edge fades in the first SrO layer, due to the destruction of long-range order in the O sublattice and the presence of interfacial O vacancies [35]. The three featured peaks (labeled as a , b , and c) for STO bulk are all observed in the second to

fourth SrO layers; however, the intensity of peak a , which is assigned to the hybridization of O $2p$ with Ti $3d(t_{2g})$, decreases from the fourth to the second SrO layer, suggesting that Ti t_{2g} orbital is partially occupied near the interface.

In summary, when GaAs is deposited on STO, As atoms are favored to be in contact with an O-deficient SrO surface to form an atomically abrupt STO/GaAs interface without surface reconstruction. The observed interface structure is consistent with the HAADF images of the STO thin film grown on GaAs substrate in the previous studies [5,6,36]. Therefore, the experimentally favorable configuration of STO/GaAs heterointerfaces is the O-deficient SrO layer in contact with the As layer, and this configuration is independent of which one is the substrate material.

B. Theoretical characterization of the interface

1. Stability of the interface structures

First-principles DFT calculations are carried out to further explore the structural and electronic properties of the STO/GaAs interfaces observed in the experiment. All the proposed interface structures are fully relaxed in the geometry optimization. As a result, some of the initial structures with different interfacial configurations turn into the same structure. In the following discussion, we focus only on the most stable geometry for each interfacial composition.

The formation energies of interface structures with different compositions are compared by the ternary phase diagrams shown in Fig. 4. The phase diagrams exhibit similar landscapes

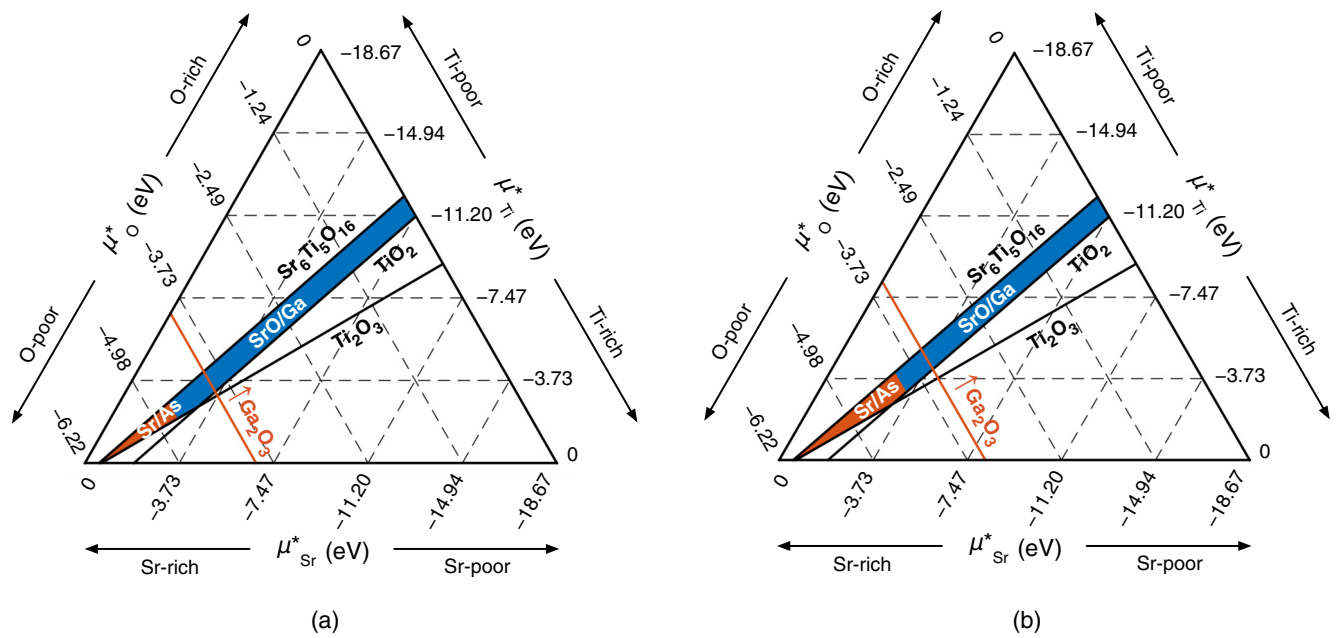


FIG. 4. The computed ternary phase diagram of the formation energies of STO/GaAs interfaces with different stoichiometries under (a) Ga-rich ($\mu_{\text{Ga}} = \mu_{\text{Ga}}^{\text{bulk}}$) and (b) As-rich ($\mu_{\text{As}} = \mu_{\text{As}}^{\text{bulk}}$) conditions. The three axes are calculated as $\mu_{\text{Sr}}^* = \mu_{\text{Sr}} - \mu_{\text{Sr}}^{\text{bulk}}$, $\mu_{\text{Ti}}^* = \mu_{\text{Ti}} - \mu_{\text{Ti}}^{\text{bulk}}$, and $\mu_{\text{O}}^* = \mu_{\text{O}} - \frac{1}{2}\mu_{\text{O}_2}^{\text{molecule}}$, where $\mu_{\text{Sr}}^{\text{bulk}}$, $\mu_{\text{Ti}}^{\text{bulk}}$, and $\mu_{\text{O}_2}^{\text{molecule}}$ are approximated by their DFT total energies. The allowed chemical potential area of stable STO without formation of other bulk materials is bounded by the solid lines corresponding to the constraints of TiO_2 , Ti_2O_3 , and Ruddlesden-Popper structure $\text{Sr}_6\text{Ti}_5\text{O}_{16}$. The region to the right of the red line denotes the formation of Ga_2O_3 .

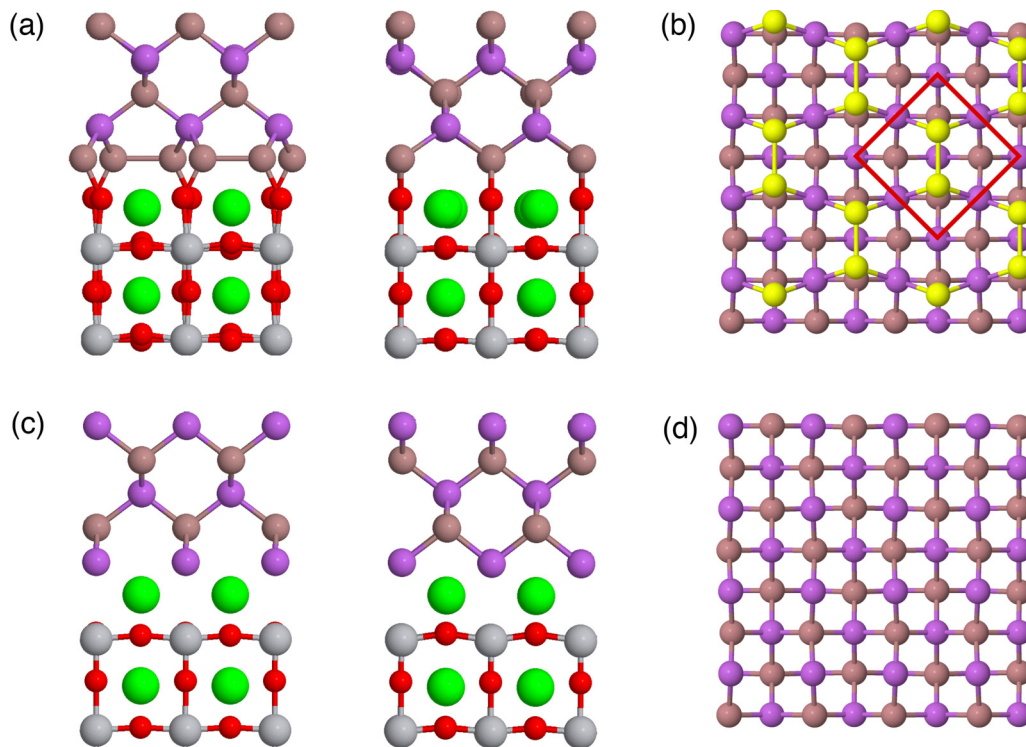


FIG. 5. The DFT-optimized structures of SrO/Ga and Sr/As interfaces. (a) The (2×2) SrO/Ga interface viewed in STO $[010]||\text{GaAs } [110]$ and STO $[100]||\text{GaAs } [1\bar{1}0]$ directions. (b) A (4×4) view of the reconstructed GaAs (001) surface at the SrO/Ga interface with the top Ga atoms highlighted. The unit cell of $c(2 \times 2)$ reconstruction is marked by a red square. (c) The (2×2) Sr/As interface viewed in STO $[010]||\text{GaAs } [110]$ and STO $[100]||\text{GaAs } [1\bar{1}0]$ directions. (d) A (4×4) view of the unreconstructed GaAs (001) surface at the Sr/As interface.

for Ga-rich and As-rich conditions. The SrO/Ga and Sr/As interfaces (the blue and red areas in the phase diagram) turn out to be the most stable structures under O-rich and O-poor conditions, respectively. The results show that a SrO layer either with or without O vacancies is favored over a TiO₂ layer at the STO/GaAs interface, which is consistent with the previous experimental findings that no Ti is observed at the interface even though a Ti thin layer was predeposited between the GaAs and the STO during the MBE growth in earlier studies [5,6]. The phase diagram illustrates a critical value of the oxygen chemical potential, $\mu_{\text{O}} = -4.67$ eV (Ga-rich) and $\mu_{\text{O}} = -4.05$ eV (As-rich), for the switching of the preferred interfacial layer from As to Ga. We also examine the formation energies using the lattice parameter of bulk GaAs ($a_{\text{GaAs}} = 5.76$ Å) for the slabs to mimic the situation of STO grown on GaAs substrate. The phase diagrams are found to be independent of the deposition sequence (i.e., GaAs on STO or STO on GaAs).

Considering the oxygen flux used in the deposition of STO, the GaAs (001) can be easily oxidized by the formation of Ga₂O₃ on the surface [12,31]. The maximal chemical potential of oxygen for an interface without forming Ga₂O₃ is calculated as $\mu_{\text{O}}^{\text{max}} = -3.94$ eV (Ga-rich) and $\mu_{\text{O}}^{\text{max}} = -3.51$ eV (As-rich). Imposing the chemical potential constraint to avoid precipitation of Ga₂O₃, the allowed region where GaAs can be epitaxially deposited on STO is restricted into a small area

in the O-poor and Sr-rich corner of the phase diagram, which is dominated by Sr/As interface. According to the calculated phase diagram, no thermodynamically stable and atomically abrupt STO/GaAs heterointerface can be obtained in the O-rich condition. Considering the normal MBE growth condition for oxygen, which is 300 to 500° C at 10⁻⁸ mbar, the allowed O chemical potential is limited to the range of -1.20 to -1.78 eV (calculated using the method in Ref. [37]), which is within the range of Ga₂O₃ formation discussed above. Therefore, when STO is directly deposited on a GaAs substrate with oxygen flux, there should, at equilibrium, always be a layer of Ga₂O₃ forming prior to the STO. In order to obtain an abrupt interface, the oxygen flux should be turned off during the growth of the interface. This kinetic inhibition of Ga₂O₃ is similar to that of SiO₂ in the STO/Si interfaces [38]. On the other hand, when depositing GaAs on STO, oxygen is mainly provided by the STO substrate; thus, the first GaAs layer is determined by the O concentration at the STO surface.

2. Atomic and electronic structures of the interfaces

In the following discussion, we mainly focus on the two energetically favorable interface structures, which are SrO/Ga and Sr/As. Figure 5 shows the relaxed structures of the two interfaces, which exhibit different patterns. In the SrO/Ga

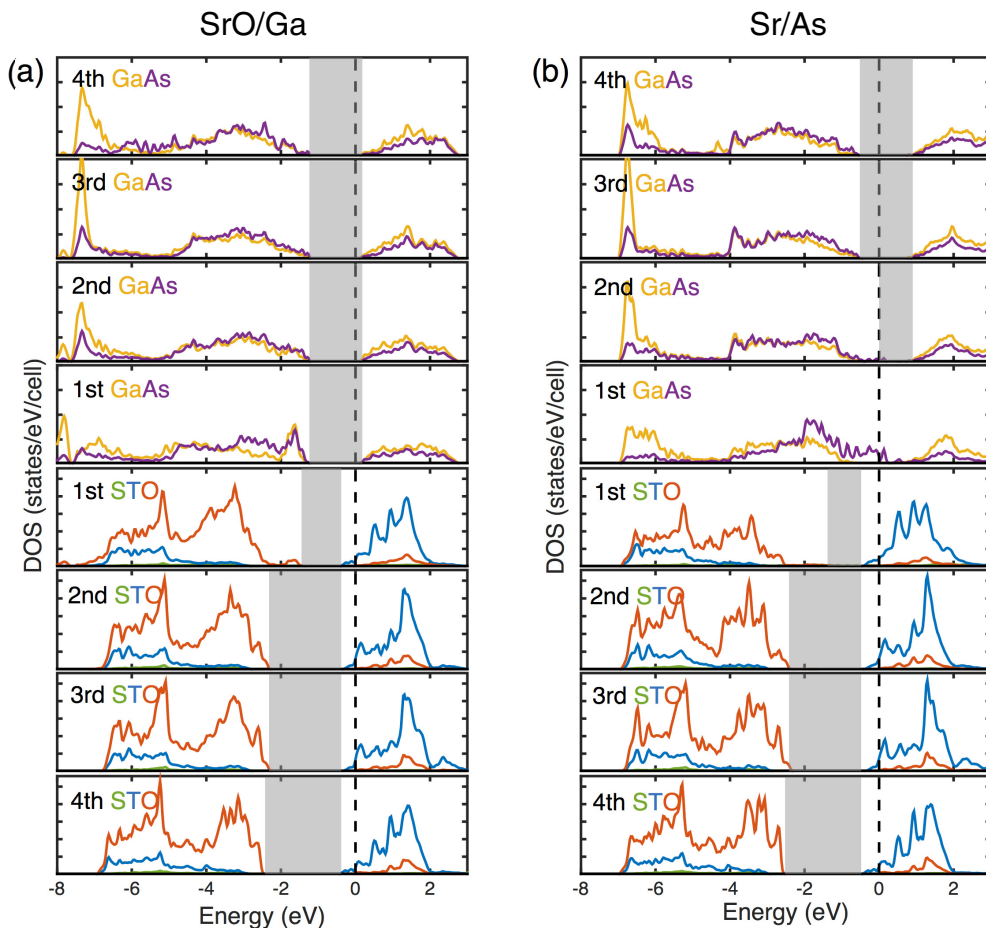


FIG. 6. Projected DOS on each element from the first to fourth STO and GaAs unit cells for (a) a SrO/Ga interface and (b) a Sr/As interface. The yellow, purple, green, blue, and red curves represent DOS on Ga, As, Sr, Ti, and O, respectively. The Fermi level is shifted to zero, and the energy gaps near the Fermi level are marked by the shaded areas.

interface structure, we find a $c(2 \times 2)$ interface reconstruction of Ga atoms by forming Ga dimers and Ga-O bonds as shown in Figs. 5(a) and 5(b). The stability of the $c(2 \times 2)$ reconstruction has been confirmed by testing larger unit cells such as (2×4) and (4×2) , known as the favorable size of GaAs surface reconstruction [39]. In the Sr/As interface structure, there is no surface reconstruction, where the (1×1) surface unit cell is preserved, and interfacial As atoms sit on the top of the Sr hollow sites (O vacancies), as shown in Figs. 5(c) and 5(d).

The STO/GaAs heterostructure can be divided into alternating (001) planes of SrO, TiO₂, Ga, and As. SrO and TiO₂ layers are charge neutral while Ga and As layers take on +3 and -3 charges, respectively. Therefore, the STO/GaAs interface has a polar discontinuity, which has to be compensated. For Ga termination, each Ga atom has $1.5e^-$ in its dangling bonds at the interface, while for SrO termination, each Sr atom can provide $2e^-$ for each O to fill the O $2p$ orbital. Thus, in the reconstructed $c(2 \times 2)$ SrO/Ga interface cell (with two atoms of each species in the surface unit cell), the electropositive elements (Ga and Sr) can provide a total of $7e^-$, while the electronegative element (O) needs only $4e^-$. Since Sr is not able to change its valence state, the interface must reconstruct to accommodate the polar discontinuity. The GaAs surface is then reconstructed by forming a Ga-Ga dimer which consumes $2e^-$ and leaves $1e^-$ [i.e., $0.5e^-$ per (1×1) unit cell]. For As termination, each As atom needs $1.5e^-$ to saturate its dangling bonds, which can be provided by the Sr atom in the Sr layer. The remaining $0.5e^-$ of the Sr atom transfers to the Ti atom in the TiO₂ layer underneath, lowering the valence of Ti from $4+$ to $3.5+$. The polar discontinuity is then accommodated by the creation of an electrical dipole in the first STO unit cell. Thus, the Sr/As interface structure is abrupt without GaAs reconstruction, which is in good agreement with the interface observed in our STEM images, and the microscopic explanation of the interfacial charge distribution can be also confirmed by the EEL spectra. The reconstruction of GaAs is found in other interface structures which are not presented in the phase diagram, such as the Sr/Ga and SrO/As interfaces (shown in the Supplemental Material [18]).

The projected densities of state (DOS) on each element in each STO and GaAs unit cell are plotted for the SrO/Ga and Sr/As interfaces, as shown in Fig. 6. Both interfaces are metallic with the Fermi level pinned to the conduction band minimum (CBM) of STO and the states at Fermi level are mainly contributed by Ti $3d$ states. In order to verify that the observed Fermi-level pinning is not an artifact of the DFT band-gap underestimation [40], we perform the PBE + U method with the effective Hubbard correction ($U = 2.0, 4.0, 6.0,$ and 8.0 eV) to Ti $3d$ states. The results show that even though the band gap of STO increases as U increases, the Fermi level remains pinned to the CBM of STO with occupied Ti $3d$ states. Therefore, the Fermi-level pinning is physically meaningful in our calculations. The details of the PBE + U calculations are presented in the Supplemental Material [18]. The localized metallic Ti $3d$ states at the CBM of STO are also found in interfaces without O vacancies, indicating that O vacancies are not the main source of these electrons. They can be attributed to the formation of two-dimensional electron gas (2DEG), which has been extensively demonstrated in the STO-based complex oxide

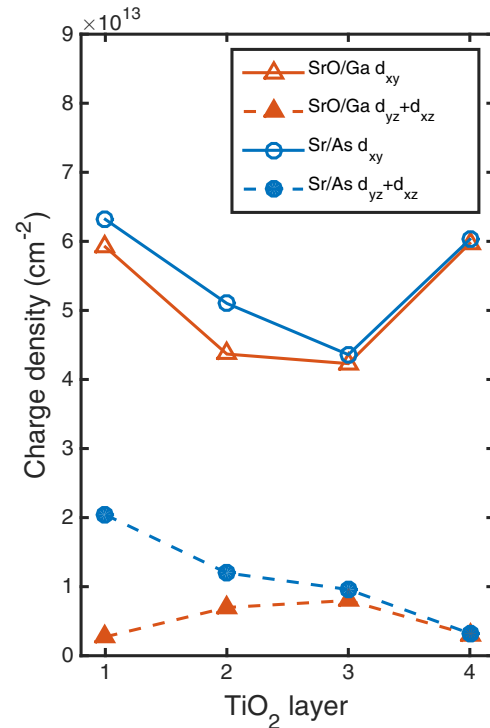


FIG. 7. Charge density of Ti d_{xy} and $d_{yz} + d_{xz}$ occupied states at the CBM of STO as a function the distance of TiO₂ layers from the interface.

heterointerfaces and vacuum-cleaved STO surface [41–49]. To further explore the 2DEG at the STO/GaAs interfaces, the charge density of the 2DEG is calculated by integrating the DOS of the Ti occupied states and plotted as a function of TiO₂ layers, as shown in Fig. 7. We can see that the occupied states in the CBM of STO exhibit a strong 2D character consisting mostly of Ti d_{xy} states. As explained before, both the SrO/Ga and the Sr/As interfaces have extra $0.5e^-$ per (1×1) unit cell, which corresponds to a charge density of $\sim 3.0 \times 10^{14}$ cm⁻², donated from the electropositive elements and transferred to the unoccupied Ti $3d$ orbitals in the first TiO₂ layer; however, the computed charge density at the interface is much lower than that value since the 2DEG can spread over several layers into the bulk region [43]. It is noteworthy that the Sr/As structure has a higher charge density than the SrO/Ga structure in the first TiO₂ layer, suggesting that O vacancies are able to enhance the 2DEG at the interface. Moreover, we find that the first and last TiO₂ layers have higher charge density than the middle layers, indicating the formation of 2DEG at both STO/GaAs interface and vacuum/STO surface.

In addition, band alignment across the SrO/Ga and Sr/As interfaces is examined, with results illustrated in Fig. 8, in order to obtain the macroscopic electronic properties of the heterostructures. For the SrO/Ga interface, the conduction and valence band offsets are calculated as $\Delta E_c = -0.15$ eV and $\Delta E_v = 1.68$ eV, corresponding to a type I heterostructure. For the Sr/As interface, the conduction and valence band offsets are obtained as $\Delta E_c = 0.57$ eV and $\Delta E_v = 2.40$ eV, corresponding to a type II heterostructure, which is in excellent agreement with the experimental values (0.6 ± 0.1 and $2.5 \pm$

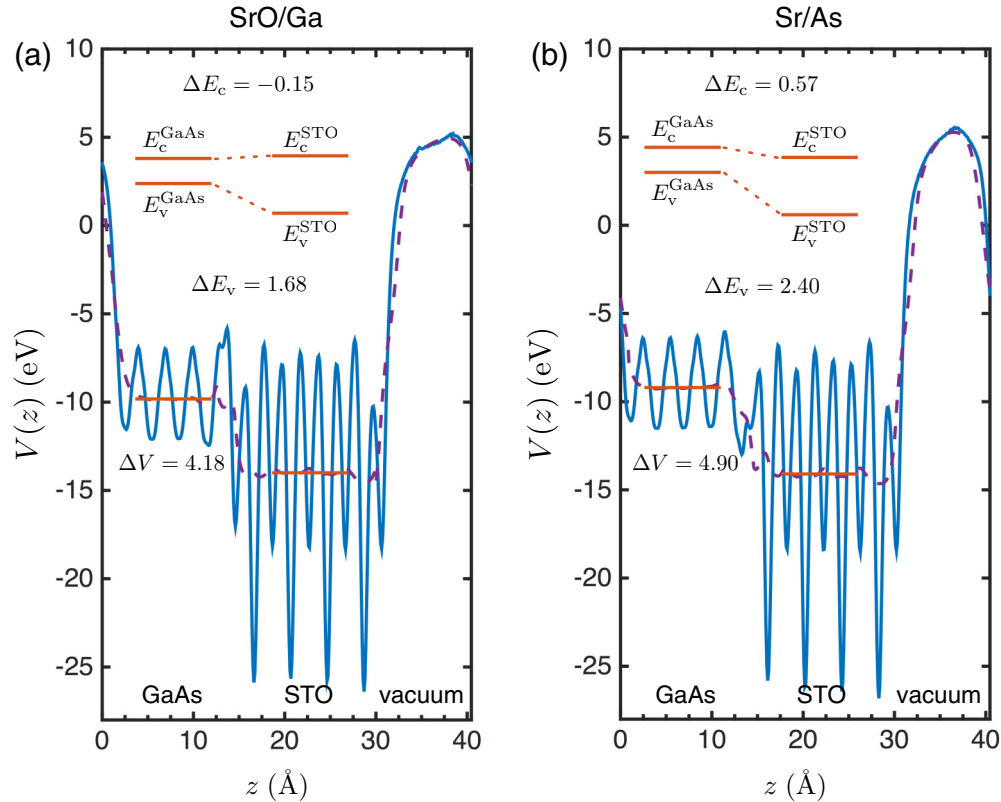


FIG. 8. Band alignment diagrams of STO/GaAs heterostructures for (a) a SrO/Ga interface and (b) a Sr/As interface. The blue solid curve represents the profile of electrostatic potential of the heterostructure along the out-of-plane direction $V(z)$, and the purple dashed curve represents the macroscopic average of the electrostatic potential. The red lines indicate the averaged values of the potential in bulklike regions and the band alignment results. The conduction and valence band offsets are determined as $\Delta E_c = E_c^{\text{GaAs}} - E_c^{\text{STO}}$ and $\Delta E_v = E_v^{\text{GaAs}} - E_v^{\text{STO}}$. ΔV stands for the difference of the averaged potential between GaAs and STO parts.

0.1 eV) [4]. The difference in band offsets between the two structures is due to the higher electrostatic potential of GaAs with respect to STO in the Sr/As interface than that in the SrO/Ga interface, as can be seen in Fig. 8.

3. Vacancies at the interfaces

From the previous discussion, we know that O vacancies play an important role in determining the structural properties of the STO/GaAs interfaces. In this section, we consider two types of interfacial defects, which are O vacancies in the first SrO layer and Ga/As vacancies in the first Ga/As layer, to gain further insights into the influence of defects on structural and electronic properties. For both Ga- and As-terminated GaAs, O vacancies are considered in the interfacial $\text{SrO}_{1-\delta}$ layer with different vacancy concentrations, $\delta = 0.25, 0.5$, and 0.75 . For SrO-terminated STO, Ga or As vacancies are created in the interfacial $\text{Ga}_{1-\theta}$ or $\text{As}_{1-\theta}$ layer with vacancy concentrations $\theta = 0.25, 0.5$, and 0.75 . For Sr-terminated STO, only As vacancies are considered in the interfacial $\text{As}_{1-\theta}$ layer with vacancy concentrations $\theta = 0.25, 0.5$, and 0.75 . Other mixed O and Ga/As vacancies are not considered in this work due to the complexity of the possible interfacial configurations.

The proposed structures are fully relaxed and their electronic structures are calculated. All the structures with vacancies are found to be energetically less stable than the

original SrO/Ga and Sr/As interfaces; nevertheless, studying the electronic behavior of these vacancies is important for understanding the interface structures and tailoring their properties. Since the metallicity of the STO/GaAs heterostructure is determined by the valence and conduction states in the interfacial layers, the projected DOS on each element in the first STO and GaAs unit cells at the interface are plotted for the considered structures with vacancies in Fig. 9. Only the $\text{SrOAs}_{0.5}$ interface exhibits semiconducting behavior with a sizable band gap; all the other interfaces are metallic. For $\text{SrO}_{1-\delta}/\text{Ga}(\text{As})$ ($\delta = 0.25, 0.5, 0.75$) interfaces, the Fermi level is always pinned to the CBM of STO. However, O vacancies induce extra dangling Ga or As states at valence band maximum (VBM) of GaAs, which reduces the band gap of GaAs at the interface. The similar pinning behavior is also reported in the STO/Si heterointerfaces [50,51]. For $\text{SrO}/\text{Ga}(\text{As})_{1-\theta}$ ($\theta = 0.25, 0.5, 0.75$) interfaces, the Fermi level can be unpinned from the CBM of STO and shifts towards the VBM as vacancy concentration increases. However, Ga and As vacancies result in extra dangling As and Ga states at Fermi level. In the case of $\text{SrO}/\text{As}_{0.5}$, the dangling states at GaAs surface can be eliminated and the Fermi level can be unpinned from STO, making the interface semiconducting. For the experimentally observed Sr/As interface with As vacancies, the Fermi level is always pinned to the CBM of STO regardless of the vacancy concentration. From these observations, we can

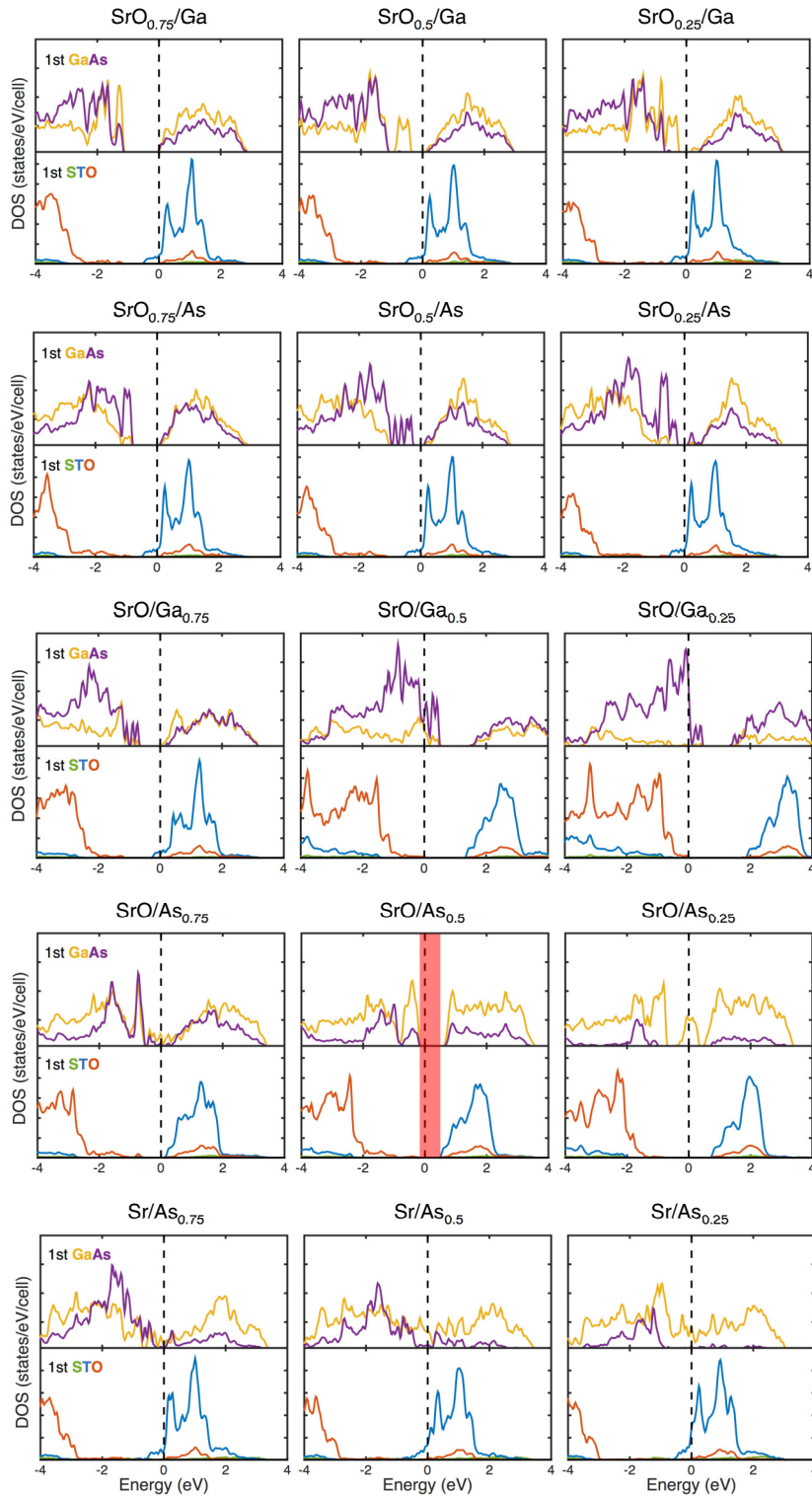


FIG. 9. Projected DOS on each element in the first STO and GaAs unit cells for the defect-induced interfaces. The Fermi level is shifted to zero. SrO/As_{0.5} is semiconducting with the band gap marked by the shaded red area.

conclude that the 2DEG in STO is intrinsic to the STO/GaAs interface and can be also contributed by O vacancies; however, it is possible for Ga or As vacancies to unpin the Fermi level from the localized 2DEG states. Both O and Ga/As vacancies will introduce more occupied Ga/As states near the Fermi level, which reduces the band gap at the interface or makes the interface metallic.

IV. SUMMARY

We study the structural and electronic properties of STO/GaAs heterointerfaces using STEM-EELS and first-principles calculations. A GaAs thick layer is grown on a STO thin film on a Si substrate by the MBE method to find out the interfacial configuration to complement the previous studies of STO thin films grown on a GaAs substrate. The

interface is characterized using atomic-resolution HAADF imaging and EELS techniques. We observe an atomically abrupt interface between STO and GaAs with the interfacial configuration of an O-deficient SrO layer in contact with an As layer, which is identical with that of a STO thin film deposited on a GaAs substrate. (2×2) structural models of various interfacial compositions with regard to SrO, TiO₂, Sr, Ti, Ga, and As terminations are constructed and fully relaxed using first-principles DFT calculations. Energetic stability of all the proposed interface structures are compared in formation energy phase diagrams. Two interfaces, with configurations SrO/Ga and Sr/As, are found to be energetically favorable under O-rich and O-poor conditions, respectively. The phase diagram also indicates that Ga-terminated GaAs surface is easily oxidized, resulting in a Ga₂O₃ interlayer. In the relaxed structure of a SrO/Ga interface, the GaAs surface is reconstructed via the formation of Ga-Ga dimers and Ga-O bonds, while the relaxed structure of Sr/As exhibits an abrupt interface without surface reconstruction, which is consistent with the experimentally observed structure. The driving force of interface reconstruction is the accommodation of interface polar discontinuity, and the presence of interfacial O vacancies is crucial to obtain an abrupt interface. Both of the two interfaces are metallic with a 2DEG of $0.5e^-$ per (1×1) unit cell localized at the bottom of Ti conduction band. Macroscopic band alignment analysis reveals that the SrO/Ga interface is a type I heterostructure while Sr/As interface is a type II heterostructure in agreement with the experiment. The

electronic properties of the STO/GaAs interfaces are further studied by examining the effects of O and Ga/As vacancies with different concentrations at the first SrO and Ga/As layers. The results show that the 2DEG in STO is intrinsic to the STO/GaAs interface and can be enhanced by O vacancies; however, it is possible for Ga or As vacancies to unpin the Fermi level from the localized 2DEG states. Experimental studies of the occurrence of the predicted 2DEG will be a subject of our future research. Our results present a detailed understanding of the structural and electronic properties of STO/GaAs heterointerfaces, which can be useful for future integration and designs of metal-oxide-semiconductor devices with advanced functions.

ACKNOWLEDGMENTS

This work was supported by the National Science Foundation (Grant No. DMR-1408427) and partially used resources of the National Energy Research Scientific Computing Center, a DOE Office of Science User Facility supported by the Office of Science of the U.S. Department of Energy under Contract No. DE-AC02-05CH11231. The acquisition of UIC JEOL JEM ARM200CF is supported by an MRI-R² grant from the National Science Foundation (Grant No. DMR-0959470). This work also made use of instruments in the Electron Microscopy Service and the High Performance Computing Clusters at Research Resources Center, UIC.

-
- [1] R. A. McKee, F. J. Walker, and M. F. Chisholm, Crystalline Oxides on Silicon: The First Five Monolayers, *Phys. Rev. Lett.* **81**, 3014 (1998).
 - [2] D. J. Smith, H. Wu, S. Lu, T. Aoki, P. Ponath, K. Fredrickson, M. D. McDaniel, E. Lin, A. B. Posadas, A. A. Demkov, J. Ekerdt, and M. R. McCartney, Recent studies of oxide-semiconductor heterostructures using aberration-corrected scanning transmission electron microscopy, *J. Mater. Res.* **32**, 912 (2017).
 - [3] Y. Liang, J. Kulik, T. C. Eschrich, R. Droopad, Z. Yu, and P. Maniar, Hetero-epitaxy of perovskite oxides on GaAs (001) by molecular beam epitaxy, *Appl. Phys. Lett.* **85**, 1217 (2004).
 - [4] Y. Liang, J. A. Curless, and D. E. McCready, Band alignment at epitaxial SrTiO₃-GaAs (001) heterojunction, *Appl. Phys. Lett.* **86**, 082905 (2005).
 - [5] R. Klie, Y. Zhu, E. Altman, and Y. Liang, Atomic structure of epitaxial SrTiO₃-GaAs (001) heterojunctions, *Appl. Phys. Lett.* **87**, 143106 (2005).
 - [6] Q. Qiao, R. F. Klie, S. Ögüt, and J. C. Idrobo, Atomic and electronic structures of SrTiO₃/GaAs heterointerfaces: An 80-kV atomic-resolution electron energy-loss spectroscopy study, *Phys. Rev. B* **85**, 165406 (2012).
 - [7] Z. P. Wu, W. Huang, K.-H. Wong, and J. H. Hao, Structural and dielectric properties of epitaxial SrTiO₃ films grown directly on GaAs substrates by laser molecular beam epitaxy, *J. Appl. Phys.* **104**, 054103 (2008).
 - [8] X. H. Wei, W. Huang, Z. B. Yang, and J. H. Hao, Interfacial and rectifying characteristic of epitaxial SrTiO_{3- δ} /GaAs *p-n* junctions, *Scr. Mater.* **65**, 323 (2011).
 - [9] R. Contreras-Guerrero, J. Veazey, J. Levy, and R. Droopad, Properties of epitaxial BaTiO₃ deposited on GaAs, *Appl. Phys. Lett.* **102**, 012907 (2013).
 - [10] L. Louahadj, R. Bachelet, P. Regreny, L. Largeau, C. Dubourdieu, and G. Saint-Girons, Molecular beam epitaxy of SrTiO₃ on GaAs(001): GaAs surface treatment and structural characterization of the oxide layer, *Thin Solid Films* **563**, 2 (2014).
 - [11] B. Meunier, R. Bachelet, G. Grenet, C. Botella, P. Regreny, L. Largeau, J. Penuelas, and G. Saint-Girons, The role of titanium at the SrTiO₃/GaAs epitaxial interface, *J. Cryst. Growth* **433**, 139 (2016).
 - [12] F. Bottin and F. Finocchi, SrTiO₃ substrates capped with a GaAs monolayer: An *ab initio* study, *Phys. Rev. B* **76**, 165427 (2007).
 - [13] J. Wang, X. Wu, and D. Bai, Stable structure and effects of the substrate Ti pre-treatment on the epitaxial growth of SrTiO₃ on GaAs, *Europhys. Lett.* **86**, 46008 (2009).
 - [14] L. Hong, S. Ögüt, and R. Klie, Transmission electron microscopic and first-principles study of SrTiO₃/GaAs heterointerfaces, *Microsc. Microanal.* **21**, 1647 (2015).
 - [15] J. Gatabi, K. Lyon, S. Rahman, M. Caro, J. Rojas-Ramirez, J. Cott-Garcia, R. Droopad, and B. Lee, Functional materials integrated on III-V semiconductors, *Microelectron. Eng.* **147**, 117 (2015).
 - [16] R. Droopad, Growth of compound semiconductor structures on patterned oxide films and process for fabricating same, US Patent No. 6,673,646 (2004).
 - [17] K. Eisenbeiser, R. Emrick, R. Droopad, Z. Yu, J. Finder, S. Rockwell, J. Holmes, C. Overgaard, and W. Ooms, GaAs

- MESFETs fabricated on Si substrates using a SrTiO₃ buffer layer, *IEEE Electron Device Lett.* **23**, 300 (2002).
- [18] See Supplemental Material at <http://link.aps.org/supplemental/10.1103/PhysRevB.96.035311> for details of the experimental and theoretical methods, which includes Refs. [19–23].
- [19] Y. Wei, X. Hu, Y. Liang, D. Jordan, B. Craig, R. Droopad, Z. Yu, A. Demkov, J. L. Edwards, Jr., and W. J. Ooms, Mechanism of cleaning Si(100) surface using Sr or SrO for the growth of crystalline SrTiO₃ films, *J. Vac. Sci. Technol. B* **20**, 1402 (2002).
- [20] R. Droopad, Z. Yu, H. Li, Y. Liang, C. Overgaard, A. Demkov, X. Zhang, K. Moore, K. Eisenbeiser, M. Hu, J. Curless, and J. Finder, Development of integrated heterostructures on silicon by MBE, *J. Cryst. Growth* **251**, 638 (2003).
- [21] T. Sands, J. Washburn, and R. Gronsky, Crystallographic relationships between GaAs, As and Ga₂O₃ at the GaAs-thermal oxide interface, *Mater. Lett.* **3**, 247 (1985).
- [22] A. Baldereschi, S. Baroni, and R. Resta, Band Offsets in Lattice-Matched Heterojunctions: A Model and First-Principles Calculations for GaAs/AlAs, *Phys. Rev. Lett.* **61**, 734 (1988).
- [23] C. G. Van de Walle and R. M. Martin, Theoretical calculations of heterojunction discontinuities in the Si/Ge system, *Phys. Rev. B* **34**, 5621 (1986).
- [24] R. F. Klie, A. Gulec, Z. Guo, T. Paulauskas, Q. Qiao, R. Tao, C. Wang, K. B. Low, A. W. Nicholls, and P. J. Phillips, The new JEOL JEM-ARM200CF at the University of Illinois at Chicago, *Cryst. Res. Technol.* **49**, 653 (2014).
- [25] G. Kresse and D. Joubert, From ultrasoft pseudopotentials to the projector augmented-wave method, *Phys. Rev. B* **59**, 1758 (1999).
- [26] G. Kresse and J. Furthmüller, Efficiency of ab-initio total energy calculations for metals and semiconductors using a plane-wave basis set, *Comput. Mater. Sci.* **6**, 15 (1996).
- [27] J. P. Perdew, K. Burke, and M. Ernzerhof, Generalized Gradient Approximation Made Simple, *Phys. Rev. Lett.* **77**, 3865 (1996).
- [28] S. B. Zhang and S.-H. Wei, Surface Energy and the Common Dangling Bond Rule for Semiconductors, *Phys. Rev. Lett.* **92**, 086102 (2004).
- [29] G.-X. Qian, R. M. Martin, and D. J. Chadi, First-principles study of the atomic reconstructions and energies of Ga- and As-stabilized GaAs(100) surfaces, *Phys. Rev. B* **38**, 7649 (1988).
- [30] C. S. Hellberg, K. E. Andersen, H. Li, P. J. Ryan, and J. C. Woicik, Structure of SrTiO₃ Films on Si, *Phys. Rev. Lett.* **108**, 166101 (2012).
- [31] H. Wieder, Perspectives on III–V compound MIS structures, *J. Vac. Sci. Technol.* **15**, 1498 (1978).
- [32] F. M. F. de Groot, M. O. Figueiredo, M. J. Basto, M. Abbate, H. Petersen, and J. C. Fuggle, *2p* X-ray absorption of titanium in minerals, *Phys. Chem. Miner.* **19**, 140 (1992).
- [33] E. Stoyanov, F. Langenhorst, and G. Steinle-Neumann, The effect of valence state and site geometry on Ti *L*_{3,2} and O *K* electron energy-loss spectra of Ti_xO_y phases, *Am. Mineral.* **92**, 577 (2007).
- [34] D. A. Muller, N. Nakagawa, A. Ohtomo, J. L. Grazul, and H. Y. Hwang, Atomic-scale imaging of nanoengineered oxygen vacancy profiles in SrTiO₃, *Nature (London)* **430**, 657 (2004).
- [35] N. Browning, J. Buban, H. Moltaji, S. Pennycook, G. Duscher, K. Johnson, R. Rodrigues, and V. Dravid, The influence of atomic structure on the formation of electrical barriers at grain boundaries in SrTiO₃, *Appl. Phys. Lett.* **74**, 2638 (1999).
- [36] Q. Qiao, Y. Zhang, R. Contreras-Guerrero, R. Droopad, S. T. Pantelides, S. J. Pennycook, S. Ogut, and R. F. Klie, Direct observation of oxygen-vacancy-enhanced polarization in a SrTiO₃-buffered ferroelectric BaTiO₃ film on GaAs, *Appl. Phys. Lett.* **107**, 201604 (2015).
- [37] K. Reuter and M. Scheffler, Composition, structure, and stability of RuO₂ (110) as a function of oxygen pressure, *Phys. Rev. B* **65**, 035406 (2001).
- [38] A. M. Kolpak and S. Ismail-Beigi, Thermodynamic stability and growth kinetics of epitaxial SrTiO₃ on silicon, *Phys. Rev. B* **83**, 165318 (2011).
- [39] M. D. Pashley, Electron counting model and its application to island structures on molecular-beam epitaxy grown GaAs(001) and ZnSe(001), *Phys. Rev. B* **40**, 10481 (1989).
- [40] C. S. Wang and W. E. Pickett, Density-Functional Theory of Excitation Spectra of Semiconductors: Application to Si, *Phys. Rev. Lett.* **51**, 597 (1983).
- [41] A. Ohtomo and H. Hwang, A high-mobility electron gas at the LaAlO₃/SrTiO₃ heterointerface, *Nature (London)* **427**, 423 (2004).
- [42] J. N. Eckstein, Oxide interfaces: Watch out for the lack of oxygen, *Nat. Mater.* **6**, 473 (2007).
- [43] Z. S. Popović, S. Satpathy, and R. M. Martin, Origin of the Two-Dimensional Electron Gas Carrier Density at the LaAlO₃ on SrTiO₃ Interface, *Phys. Rev. Lett.* **101**, 256801 (2008).
- [44] N. Nakagawa, H. Y. Hwang, and D. A. Muller, Why some interfaces cannot be sharp, *Nat. Mater.* **5**, 204 (2006).
- [45] S. Thiel, G. Hammerl, A. Schmehl, C. Schneider, and J. Mannhart, Tunable quasi-two-dimensional electron gases in oxide heterostructures, *Science* **313**, 1942 (2006).
- [46] A. Brinkman, M. Huijben, M. Van Zalk, J. Huijben, U. Zeitler, J. Maan, W. Van der Wiel, G. Rijnders, D. Blank, and H. Hilgenkamp, Magnetic effects at the interface between non-magnetic oxides, *Nat. Mater.* **6**, 493 (2007).
- [47] W. Siemons, G. Koster, H. Yamamoto, W. A. Harrison, G. Lucovsky, T. H. Geballe, D. H. A. Blank, and M. R. Beasley, Origin of Charge Density at LaAlO₃ on SrTiO₃ Heterointerfaces: Possibility of Intrinsic Doping, *Phys. Rev. Lett.* **98**, 196802 (2007).
- [48] A. Kalabukhov, R. Gunnarsson, J. Börjesson, E. Olsson, T. Claeson, and D. Winkler, Effect of oxygen vacancies in the SrTiO₃ substrate on the electrical properties of the LaAlO₃/SrTiO₃ interface, *Phys. Rev. B* **75**, 121404 (2007).
- [49] A. Santander-Syro, O. Copie, T. Kondo, F. Fortuna, S. Pailhes, R. Weht, X. Qiu, F. Bertran, A. Nicolaou, A. Taleb-Ibrahimi *et al.*, Two-dimensional electron gas with universal subbands at the surface of SrTiO₃, *Nature (London)* **469**, 189 (2011).
- [50] I. N. Yakovkin and M. Gutowski, SrTiO₃/Si (001) epitaxial interface: A density functional theory study, *Phys. Rev. B* **70**, 165319 (2004).
- [51] A. M. Kolpak and S. Ismail-Beigi, Interface structure and film polarization in epitaxial SrTiO₃/Si(001), *Phys. Rev. B* **85**, 195318 (2012).